# X-ray Absorption Spectroscopy Study of Novel Inorganic−organic Hybrid Ferromagnetic Cu−pyz−[M(CN)$_8$]$^{3−}$ Assemblies

Olaf Stefańczyk,*,[†] Robert Podgajny,[†] Tomasz Korzeniak,[†] Michał Rams,[‡] Marcin Kozieł,[†] Wiesław Łasocha,[†] Dariusz A. Zając,[§,‖] and Barbara Sieklucka*,[†]

[†]Faculty of Chemistry, Jagiellonian University, Ingardena 3, 30-060 Kraków, Poland

[‡]M. Smoluchowski Institute of Physics, Jagiellonian University, Reymonta 4, 30-059 Kraków, Poland

[§]Helmholtz-Zentrum Berlin für Materialien und Energie GmbH, Institut of Solar Fuels and Energy Storage Materials, Hahn Meitner Platz 1, D-14109 Berlin, Germany

[‖]HASYLAB, Deutsches Elektronen-Synchrotron A Research Centre of the Helmholtz Association, Notkestrasse 85, 22607 Hamburg, Germany

S *Supporting Information*

ABSTRACT: We present a unique interpretation of X-ray absorption spectroscopy (XAS) spectra at Cu:K, W:L$_3$, and Mo:K edges of structurally related magnetic Cu^{II}−[M^V(CN)$_8$]$^{3−}$ compounds. The approach results in description of the structure of novel three-dimensional (3-D) Cu$^{II}_3$(pyz)-[M^V(CN)$_8$]$_2$·xH$_2$O, M = W (**1**), Mo, (**2**) polymers. Assemblies **1** and **2** represent hybrid inorganic−organic compounds built of {Cu^{II}[W^V(CN)$_8$]$^−$}$_n$ double-layers linked by cyanido-bridged {Cu^{II}−(μ-pyz)$^{2+}$}$_n$ chains. These Cu^{II}−M^V systems reveal long-range magnetic ordering with T_c of 43 and 37 K for **1** and **2**, respectively. The presence of the 3-D coordination networks and 8 cyanido-bridges at M^V centers leads to the highest Curie temperatures and widest hysteresis loops among Cu^{II}−[M^V(CN)$_8$]$^{3−}$ systems.
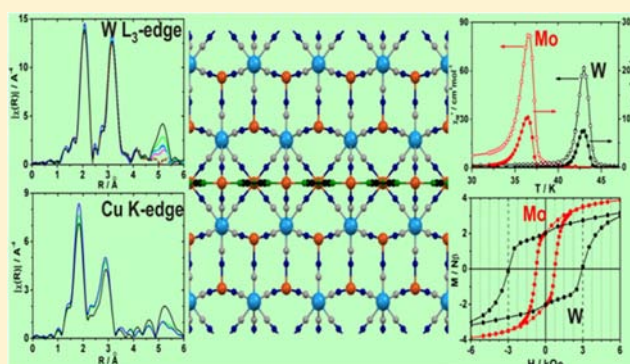
INTRODUCTION

Several interesting families of {Cu−[M(CN)$_8$]$^{n−}$} coordination skeletons could be recognized because of their intriguing magnetic, optical, and photomagnetic properties.[1] One of the most appealing are systematically observed {Cu^{II}[W^V(CN)$_8$]$^−$}$_n$ cyanide-bridged double layers, which could be either stabilized by cationic sheets of dienH$_3^{3+}$ (dien = diethylenetriamine),[2a] tetrenH$_5^{5+}$ (tetren = tetraethylenepentaamine),[2a,b] or Cs^{+3} or linked by the additional CN−Cu−NC linkages into a three-dimensional (3-D) coordination framework.[4] Their ordering temperatures reach up to 40 K with the noticeable magnetic hysteresis loops at low temperatures. Several physical reports presented the complete characterization of this class of compounds, revealing pressure and field effects on the ordering, muon relaxation characteristics, the XY type magnetic anisotropy, and the very rare type of vortex Berezinsky−Kosterlitz−Thouless (BKT) transition from the paramagnetic phase to the ordered phase for layered {(tetrenH$_5$)$_{0.8}$Cu$^{II}_4$[Mo^V(CN)$_8$]$_4$·7.2H$_2$O}$_n$.[5] To extend knowledge about the magneto−structural correlation and to gain high T_c in organic−inorganic hybrid Cu−[M(CN)$_8$]$^{3−}$ assemblies, we investigated the reaction of [M(CN)$_8$]$^{3−}$ with Cu^{II} in the presence of pyrazine at low pH. We have exploited pyrazine's ability to form local and extended coordination {M^{II}−(μ-

pyz)$_m^{2+}$}$_n$ (m = 1/2, 1, 2, 3) motifs with divalent d metal cations,[6] which issued magnetic exchange coupling,[6f] as well as room temperature spin−crossover (SCO) and chemical vapor sensitivity[7] or second order magneto−optical effects.[6g] Herein, we present two novel hybrid magnetic networks Cu$^{II}_3$(pyz)-[W^V(CN)$_8$]$_2$ (**1**) (T_c = 43 K) and Cu$^{II}_3$(pyz)-[Mo^V(CN)$_8$]$_2$·3.5H$_2$O (**2**) (T_c = 37 K) built by CN$^−$−bridged {Cu^{II}[W^V(CN)$_8$]$^−$}$_n$ double-layers and {Cu^{II}−(μ-pyz)$^{2+}$}$_n$ chains. The structural (powder X-ray diffraction, XANES/EXAFS spectroscopies[4,8]) and magnetic studies allow for magneto−structural correlation of **1**, **2** and the related {Cu−[M(CN)$_8$]$^{n−}$} polynuclear compounds.

EXPERIMENTAL SECTION

Materials. Cupric nitrate, pyrazine, and HCOOH were purchased from commercial sources (Sigma-Aldrich, Lach-Ner) and used as received. Sodium octacyanidotungstate(V) **Na$_3$W**, cesium octacyanidomolybdate(V)[9] and Cu$^{II}_{2.44}${Cu$_4$[W^V(CN)$_8$]$_{3.12}$-[W^{IV}(CN)$_8$]$_{0.88}$]·5H$_2$O **Cu$_{2.44}$W**,[4] Cu$^{II}_3$[Mo^V(CN)$_8$]$_2$·3H$_2$O **CuMo**,[10] (dienH$_3$){Cu^{II}[W^V(CN)$_8$]}$_3$·4H$_2$O **dienCuW**,[2a] {(tetrenH$_5$)$_{0.8}$Cu$^{II}_4$-[W^V(CN)$_8$]$_4$·7.2H$_2$O}$_n$ **tetrenCuW**,[2b] Cu$^{II}_2$(Hpyr)$_5$(H$_2$O)-[W^V(CN)$_8$](NO$_3$)·H$_2$O (Hpyr = pyrazole) **pyrCuW**,[11] and

$[Cu^{II}(bpy)_2]_2[Cu^{II}(bpy)_2][W^V(CN)_8]_2\cdot4H_2O$ (bpy = 2,2′−bipyridine) **bpyCuW**,[12] as references for XAS measurements have been synthesized according to the published procedures. The synthetic procedures involving $[M(CN)_8]^{3-}$ ions have been performed in the dark room to avoid photoreactivity. Additionally, in the case of $[Mo(CN)_8]^{3-}$ ions, the syntheses have been performed at 4 °C.

Synthesis of $Cu^{II}_3(pyz)[W^V(CN)_8]_2$ (1). To the solution containing $Cu(NO_3)_2\cdot3H_2O$ (242 mg, 1 mmol) and HCOOH (76 μL, 1.7 mmol) in 10 mL of H_2O the solution of pyrazine (80 mg, 1 mmol, 15 mL of H_2O) was slowly added, followed by dropwise addition of solution containing $Na_3[W(CN)_8]\cdot4H_2O$ (0.352 g, 0.66 mmol, 25 mL of H_2O) upon vigorous stirring. Polycrystalline green powder was formed immediately and filtered under vacuum. Yield: 310.5 mg (89%). Elementary Anal. Calcd for $C_{20}H_4Cu_3N_{18}W_2$: C, 22.78%; H, 0.38%; N, 23.90%. Found: C, 22.93%; H, 0.26%; N, 23.60%. IR spectrum in $\nu(CN)$ region (cm^{-1}): 2212 m(sh), 2199s, 2164 m.

Synthesis of $Cu^{II}_3(pyz)[Mo^V(CN)_8]_2\cdot3.5H_2O$ (2). The compound was obtained in a similar procedure to that of **1**, but $Cs_3[Mo(CN)_8]\cdot4H_2O$ (512 mg, 0.66 mmol, 25 mL of H_2O) instead of $Na_3[W(CN)_8]\cdot4H_2O$ was used. Polycrystalline green precipitate was formed immediately. Product was filtered in dry argon atmosphere and stored at 4 °C in closed Schlenk vessel. Yield: 265.3 mg (85%). Elementary Anal. Calcd for $C_{20}H_{11}Cu_3Mo_2N_{18}O_{3.5}$: C, 25.50%; H, 1.18%; N, 26.77%. Found: C, 25.91%; H, 1.19%; N, 26.51%. IR spectrum in $\nu(CN)$ region (cm^{-1}): 2212 m(sh), 2199s, 2164s.

Powder X-ray Crystallography. Diffraction measurements for **1** and **2** were performed on a PANanalytical X'Pert PRO MPD diffractometer with a Bragg−Brentano geometry using CuKα radiation $(\lambda = 1.54178$ Å). The patterns were collected at 298 K between 4° and 60° 2θ angle. Powder X-ray diffraction patterns for references were generated with Mercury software.[13]

Physical Techniques. Infrared spectra were recorded in the range of 600−4000 cm^{-1} using a Thermo Scientific Nicolet iS5 spectrometer equipped with iD5 ATR−Diamond. Elemental analyses (C, H, N) were performed on ELEMENTAR Vario Micro Cube CHNS instruments. Thermogravimetric data in the temperature range 25−400 °C were collected on a Mettler Toledo TGA/SDTA 851e microthermogravimeter equipped with QMS Thermostar GSD 300 T Balzers at heating rate of 9 °C min^{-1} in Ar atmosphere. The X-ray Absorption Spectroscopy (XAS) experiments have been performed in the HASYLAB (DESY, Germany) at Doris III storage ring at experiment station CEMO, with bending magnet source. The Si(111) (Cu:K and W:L_3 edges) or Si(311) (Mo:K edge) monochromator has been used. Data has been collected at 77 K, in transmission mode, simultaneously with the reference foil (Cu metallic foil 5 μm) as the energy standard. The signals have been acquired from ionization chambers, filled with proper gases to obtain 10%, 50%, and 100% of absorption, for the first, second, and third chamber, respectively. The samples have been prepared in the form of pellets, mixed with cellulose. Their masses have been chosen to be optimized for each edge, to the edge jump for K edges (or the height of the white line for L edges) equal 1. The stability of the samples under X-ray exposure has been also studied using QEXAFS, and no changes have been observed in the time scale of 2 h. There are also no visible changes in the sample in the place of beam before and after the exposure. The X-ray absorption spectra in the EXAFS and XANES range have been elaborated using ATHENA software.[14] Magnetic measurements for **1** and **2** were performed using a Quantum Design SQUID magnetometer MPMS5-XL. All experimental magnetic data were corrected for the diamagnetism of the sample holders and of the constituent atoms (Pascal's tables).

■ RESULTS

Synthesis. The self-assembly of the copper(II) ions, pyrazine, and octacyanidometallate(V) in Cu/pyz/$[M(CN)_8]^{3-}$ = 3/9/2 ratio resulted in the formation of two novel compounds: $Cu_3(pyz)[M(CN)_8]_2\cdot xH_2O$ (M = W, x = 0 (**1**); M = Mo, x = 3.5 (**2**)). During synthesis of **1** and **2**, HCOOH was applied to obtain water-soluble precursor copper(II)

complexes with pyrazine and formate anions.[15] Addition of octacyanidometallate(V) ion resulted in formation of the appropriate products via substitution of anions present in Cu^{II}−pyz coordination polymers with $[M(CN)_8]^{3-}$ moieties.

Structural Investigations. All attempts to obtain single crystals suitable for single crystal X-ray diffraction analysis were unsuccessful; however, the compounds were characterized by the powder X-ray diffraction method. The powder diffraction patterns of **1** and **2** are presented in Figure 1. Indexing of the
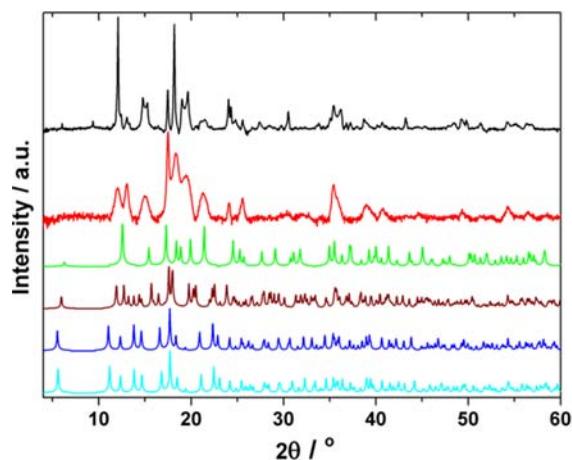

Figure 1. Powder diffraction patterns of **1** (black) and **2** (red), and calculated diffraction patterns for the reference compounds: **$Cu_{2.44}W$** (green), **CsCuW** (brown), **dienCuW** (blue), and **tetrenCuW** (cyan).

patterns yielded no reliable result; however, several conclusions can be made based on the diffraction patterns only. In case of the molybdenum analogue, broadening of most peaks has been observed, probably because of the small size of the crystallites in particular crystallographic directions or significant disorder in the structure. Despite of broad peaks in the pattern of **2** it matches well the pattern of **1**. Therefore, we conclude that **1** and **2** are isostructural. Moreover, the similarity of X-ray patterns for **1** and **2** with those of the reference compounds, $Cu^{II}_{2.44}\{Cu^{II}[W^V(CN)_8]_{3.12}[W^{IV}(CN)_8]_{0.88}\}\cdot5H_2O$ **$Cu_{2.44}W$**,[4] $Cs^ICu^{II}[W^V(CN)_8]\cdot0.5H_2O$ **CsCuW**,[3] $(dienH_3)\{Cu^{II}[W^V(CN)_8]\}_3\cdot4H_2O$ **dienCuW**,[2a] $\{(tetrenH_5)_{0.8}Cu^{II}_4[W^V(CN)_8]_4\cdot7.2H_2O\}_n$ **tetrenCuW**,[2b] indicate a double-layered CN^--bridged $\{Cu^{II}[W^V(CN)_8]^-\}_n$ type of coordination skeleton. For layered structures the interlayer distance can be extracted from the PXRD pattern directly (eq 1). This distance should be attributed to one of the first, distinct Bragg peaks.

$$d_{hkl} = \frac{n\lambda}{2\sin\theta} \tag{1}$$

Such approach is valid for two-dimensional (2-D) structures that fulfill three conditions: (a) the distance between layers is the largest or one of the largest interplanar distance, (b) the layers consist of heavy atoms in comparison to the space between layers to produce a high structure factor in the perpendicular direction, (c) the peak attributed to interlayer distance is not absent due to symmetry or disorder. By comparison with other, previously known layered structures of similar type (Figure 1), we observed that the interlayer distance is attributed to the first Bragg peak (Supporting Information, Table S2). For **1** this distance equals 14.6 ± 0.9 Å. For **2** this value should be similar because of isostructural character.

X-ray Absorption Spectroscopy (XAS) Studies. The XAS spectra and their first derivatives in the Cu:K edge XANES range for **1**, **2** as well as for the reference samples of metallic **Cu** (Cu foil), **CuBr**, **CuCl₂**, **Cu₂.₄₄W**, **CuMo**, and **dienCuW** are presented in Figure 2. The edge energy of Cu metallic foil has
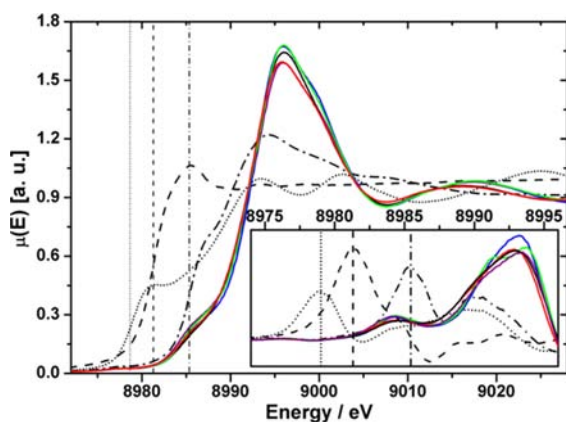

Figure 2. Normalized Cu:K edge XAS spectra in the XANES range for: **1** (black), **2** (red), **Cu₂.₄₄W** (green), **CuMo** (purple), **dienCuW** (blue), and references of metallic **Cu** (dot), **CuBr** (dash), and **CuCl₂** (dash dot). **Inset:** first derivative of the XANES signal. Perpendicular lines represent estimated oxidation states of copper: Cu(0) (dots), Cu(I) (dash) and Cu(II) (dash dot).

been defined as the first maximum of the first derivative of XANES spectra at 8979 eV. Edge energies of the investigated samples are estimated in two ways: (i) as the first maximum of the first derivative of XANES spectra (FMFD), and (ii) as the energy point at the half height of the normalized spectra (HHE) (Supporting Information, Table S3). It has to be noted that both methods (FMFD and HHE) yield the values of the edge positions very close to the edge position of $CuCl_2$, confirming oxidation state of copper ions in **1** and **2** samples very close to 2+. The investigations performed for other Cu–[M(CN)₈]³⁻ systems: **Cu₂.₄₄W**, **CuMo**, and **dienCuW**, yielded the edge energies for Cu^{II}–M^V assemblies similar to **1** and **2**, confirming the oxidation state of copper centers close to 2+. In all cases, the estimated oxidation states of the Cu centers are consistent with the values from the formula.

The W:L₃ edge XANES spectra for **1**, **Cu₂.₄₄W**, **dienCuW**, **tetrenCuW**, **pyrCuW**, **bpyCuW**, and **Na₃W** are presented in

Supporting Information, Figure S1. The Mo:K edge for **2** and **CuMo** are presented in Supporting Information, Figures S2. The edge positions for all compounds are located at the energy of 20014 and 10210 eV for Mo:K and W:L₃ edges, respectively, and are in the connection with energies of 20000 and 10207 eV for metallic references Mo and W samples.

The EXAFS functions $\chi(k)$ were obtained from the experimental spectra by subtraction of the atomic absorption background, approximated by a spline function with the R_{bkg} parameter of 1.0 Å for Cu:K, W:L₃, and Mo:K edges. The $k^3 \times \chi(k)$ functions of **1**, **2**, and reference complexes are presented in Supporting Information, Figure S3−S6. They were Fourier transformed using the Hanning window in the range of $k = 3–13$ Å⁻¹ taking into account the phase shift to the excited atom.

The EXAFS functions $\chi(R)$ obtained from the W:L₃ edge spectra of **1**, and references: **Cu₂.₄₄W**, **dienCuW**, **tetrenCuW**, **pyrCuW**, **bpyCuW**, and **Na₃W** are presented in Figure 3 left. They reveal two dominant peaks at about 2.1 and 3.2 Å and a weaker one with maximum at 5.1 Å. Each of them correspond to three consecutive coordination spheres of tungsten (Table 1). The first two peaks of $\chi(R)$ function can be assigned to the carbon and nitrogen atoms of cyanide. The positions of both peaks agree well with W−C and W−N distance of 2.15 and 3.3 Å from single crystal X-ray diffraction of reference compounds (Supporting Information, Table S4 and Figure S7). Moreover, very similar shape of peaks at 2.1 and 3.2 Å for all compounds suggest that energy scatters in the same way, and despite the contribution of multipath in EXAFS spectra, these results can be compared qualitatively. The last peak around 5.1 Å is related directly to the cyanido-bridged copper(II) centers. This distance is in a reasonable agreement with the value of 5.3 Å taken from single crystal X-ray diffraction and is proven by the comparison with the EXAFS spectrum of the precursor material, where only C and N peaks are visible. The reason for the observed difference is an approximation used in the phase correction in the elaboration of the spectra and a relatively large contribution of multipaths in spectra.

Noticeably, the intensity of the peak at 5.1 Å for the references assemblies decreases in the order **Cu₂.₄₄W** > **dienCuW** = **tetrenCuW** > **pyrCuW** > **bpyCuW** > **Na₃W** correlating with the average number of Cu−NC−W linkages of 7, 5, 5, 4, 1.5, and 0, respectively. The highest intensity of this peak for **1** suggests that the average number of bridging cyanido ligands should exceed seven cyanido-bridges, yet could not be
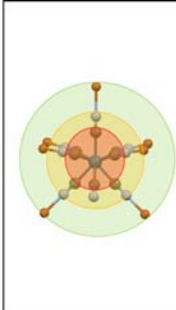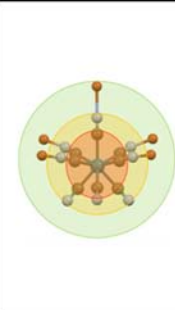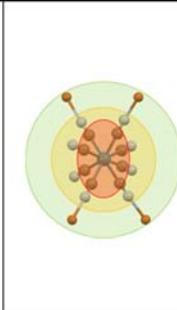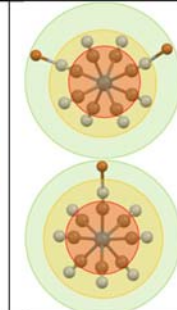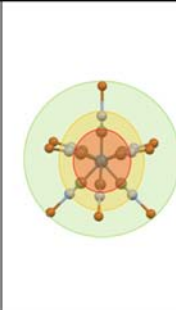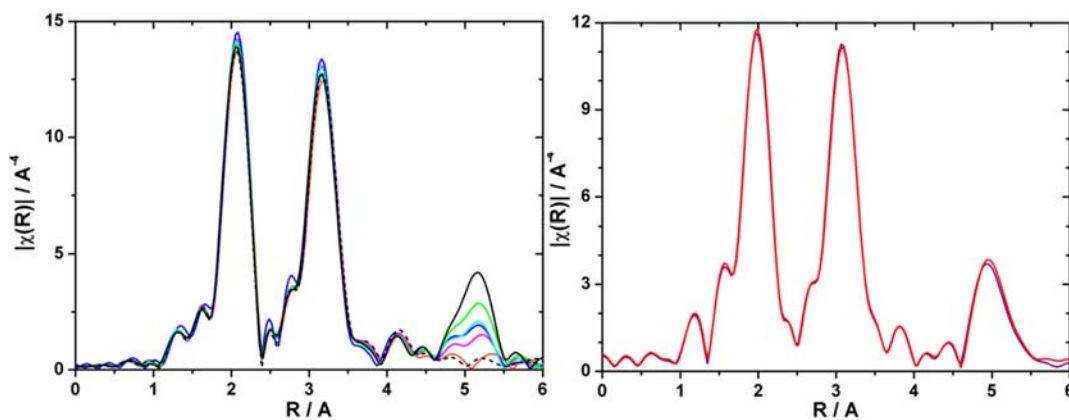

Figure 3. Left: the Fourier transform of the W:L₃ edge (EXAFS spectra) for **1** (black), **Cu₂.₄₄W** (green), **dienCuW** (blue), **tetrenCuW** (cyan), **pyrCuW** (magenta), **bpyCuW** (orange), and **Na₃W** (dotted line). Right: the Fourier transform of the Mo:K edge for **2** (red) and **CuMo** (purple).

Table 1. First (Red), Second (Yellow), and Third (Green) Coordination Sphere of Tungsten Centers of the Reference Compounds: Cu$_{2.44}$W, dienCuW, tetrenCuW, pyrCuW, and bpyCuW, Together with Those of 1

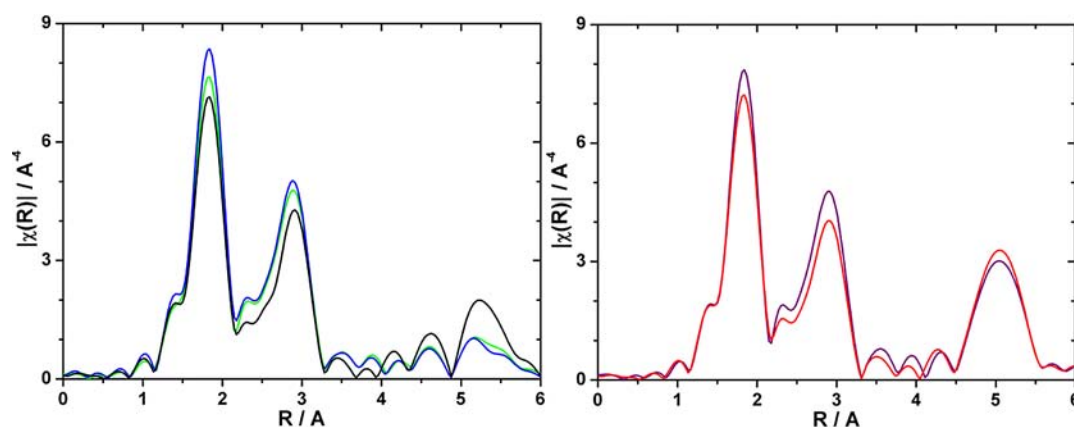|	Cu$_{2.44}$W	dienCuW and tetrenCuW	pyrCuW	bpyCuW	1
Sphere	Number of atoms in sphere				
1st	8	8	8	8	8
2nd	8	8	8	8	8
3rd	7	5	4	2+1	8

Figure 4. Left: the Fourier transform of the Cu:K edge (EXAFS spectra) for **1** (black), **Cu$_{2.44}$W** (green), and **dienCuW** (blue). Right: the Fourier transform of the Cu:K edge for **2** (red) and **CuMo** (magenta).

larger than eight. The coordination shells of tungsten of **1** are presented on the right side of Table 1.

The χ(R) functions of **2** and **CuMo** (Figure 3 right) obtained from the Mo:K edge spectra exhibit very similar shape to the χ(R) functions obtained for W:L$_3$ edge. They reveal two dominant peaks at 2.0 and 3.1 Å and a three times smaller peak at 5.0 Å, corresponding to the presence of C, N, and Cu atoms, respectively. The positions of the two first maxima agree well with distances from X-ray diffraction for other compounds with [Mo(CN)$_8$]$^{3-}$, but the position of the third peak is shorter than expected value of 5.3 Å. This difference is connected with an approximation used in the phase correction and strong contribution of multipaths. The magnitudes of all peaks for **2** and **CuMo** are comparable suggesting analogous local structure of both compounds, with the eight of Mo−CN−Cu linkages.

The local coordination of copper centers in **1**, **Cu$_{2.44}$W**, and **dienCuW** were estimated from the intensity and position of peaks in the EXAFS functions χ(R) obtained for the Cu:K edge. This functions exhibit a few dominant peaks at about 1.9, 2.9, and 5.2 Å for Cu−W systems (Figure 4 left). The structural parameters for **Cu$_{2.44}$W** and **dienCuW** from single crystals X-ray measurements are collected in Supporting Information, Table S5 and Figure S8. The first peak at 1.9 Å is directly connected with the coordination number of the copper center.

This coordination sphere consists of nitrogen atoms of CN$^-$ and bridging pyrazine molecules as well as oxygen atoms of coordinated water molecules (Table 2). The second coordination sphere of copper represented by the peak at 2.9 Å corresponds to carbon atom of cyanido ligand, two carbon atoms of pyrazine, and oxygen atoms of H−bond water molecules. The magnitude of both peaks for Cu−W systems decreases in series: **dienCuW** > **Cu$_{2.44}$W** > **1**. Interpretation of the magnitude of these peaks is impossible because of the presence of disorder in space between double-layers connected with partially occupied cyanido-bridges and coordination water and pyrazine molecules. The third peak at 5.1 Å is attributed to the cyanido-bridged tungsten atoms and carbon atoms of pyrazine. The most intense signal is observed for **1**, while **Cu$_{2.44}$W** and **dienCuW** are less intense. This observation suggests that all investigated compounds are surrounded in same way in the third sphere but **1** with the strongest signal of **1** due to coordinated pyrazine with higher number of atoms contributing to the resonance. The coordination shells of copper of **1** are presented on the right side of Table 2.

The same shape of χ(R) functions with peaks at about 1.9, 2.9, and 5.0 Å is observed for Cu−Mo systems (Figure 4 right). The first two peaks correspond to nitrogen atoms of CN$^-$ and bridging pyrazine, oxygen of coordination H$_2$O for first one and

Table 2. First (Red), Second (Yellow), and Third (Green) Coordination Sphere of Copper Centers of Cu$_{2.44}$W and dienCuW, Together with Those of 1

Sphere	Number of atoms in sphere			The magnitudes of peaks
	Cu$_{2.44}$W	**dienCuW**	**1**	
1st	2x5 + 4^a	2x5	2x5 + 6^a	dienCuW > Cu$_{2.44}$W > 1
2nd	2x6 + 6^a	2x6	2x5 + 8^a	dienCuW > Cu$_{2.44}$W > 1
3rd	2x5 + 4^a	2x5	2x5 + 8^a	1 > Cu$_{2.44}$W = dienCuW

^{a}Partially occupied atoms.

carbon atoms of CN$^-$ and pyrazine, oxygen of H−bonded water. The third peak is related only to the cyanido-bridged molybdenum and carbon atoms of pyrazine. The magnitude of this peak is higher for **2** than for **CuMo** because of the presence of bridging pyrazine in structure of **2**. These conclusions are consistent with conclusions for Cu−W systems.

TGA/QMS Analyses. The thermal decomposition of the anhydrous **1** occurs in three steps, starting at 170 °C (Figure 5). The first step between 170 and 270 °C corresponds to loss of terminal CN$^-$ (m/z = 26.18 (CN$^+$), 27.18 (HCN$^+$)). The mass loss value of 4.8% observed in this step agrees well with the calculated value of 4.9% (loss of two CN$^-$). Elimination of the pyrazine (m/z = 26.18 (CN$^+$), 27.18 (HCN$^+$), 53.25 (HC$_2$N$_2$$^+$), 80.22 (H$_4C_4N_2$$^+$)) and CN$^-$ (m/z = 26.18 (CN$^+$), 27.18 (HCN$^+$)) ligands take place in the temperature range
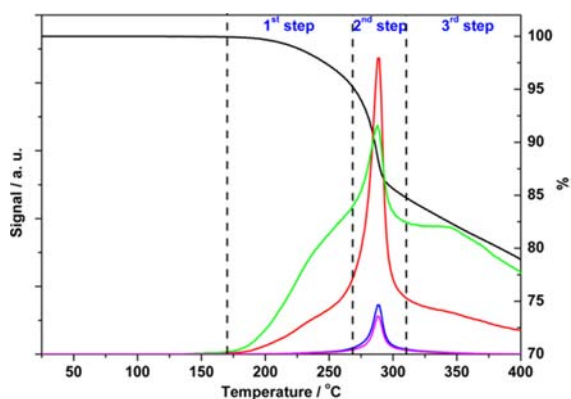

Figure 5. TGA (black) coupled with QMS analyses for **1**. m/z = 26.18 (red), 27.18 (green), 53.25 (blue), 80.22 (magenta).

270−310 °C.[6c,16] In this stage the mass value is reduced by the next 10.3% (calcd 10.1% for loss of pyrazine and CN$^-$). The maximum of pyrazine loss was obtained in 280 °C. Further increase of temperature results in the overall weight loss of 21% at 400 °C.

Structural Model of 1 and 2. The molecular structure of both systems was gained from PXRD and XAS spectroscopy as well as from the standard physical techniques (EA, IR, TGA/QMS). Infrared bands in ν(CN) region in range 2300−2000 cm^{-1} confirmed the presence of bridging [M^V(CN)$_8$]$^{3-}$ (M = W, Mo) moieties. The shift of bands to the higher energy in the fingerprint region below 1800 cm^{-1} reveal the presence of bridging pyrazine, in comparison to free ligand (Supporting Information, Table S1, Figure S9−S11). The absence of water molecules and the presence of pyrazine for **1** was also confirmed by thermogravimetric measurements. To examine the molecular structure of **1** and **2** we used X-ray absorption spectroscopy in the EXAFS range. The interpretation of data for W:L$_3$, Mo:K, and Cu:K edge results in a structural model for **1** and **2** (Figure 6). The proposed model assumes that the bilayers {Cu$_2$[M(CN)$_8$]$_2$}$^{2- \; 2-4}$ are linked via the cyanido-bridges from [M(CN)$_8$]$^{3-}$ to the copper(II) pyrazine chains. Inter-layer pyrazine molecules, CN$^-$-bridges, and Cu(II) centers are disordered, which strongly affects on quality of powder X-ray diffraction patterns.

Magnetic Properties. The fit of $\chi_M^{-1}(T)$ data to the Curie−Weiss law (Figure 7) in the 150−300 K temperature range leads to the Weiss constants θ equal to 65(1) and 60(1) K for **1** and **2**, respectively. The large and positive θ values imply that the magnetic interaction through the Cu^{II}−NC−M^V bridges is of ferromagnetic nature. The values of the Curie constants 2.13(1) and 2.11(1) cm^3 K mol^{-1} for **1** and **2**,
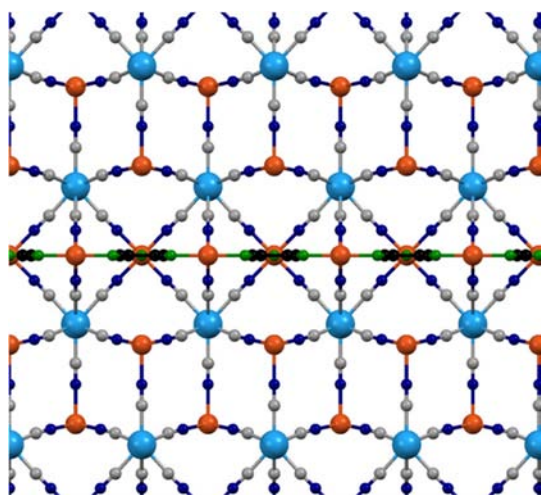
Figure 6. Structural model of **1** and **2**. Colors used: W (blue); Cu (orange); C_{CN} (gray); and N_{CN} (navy) in CN^- bridges; C_{pyz} (black) and N_{pyz} (green) in delocalized pyrazine bridges.
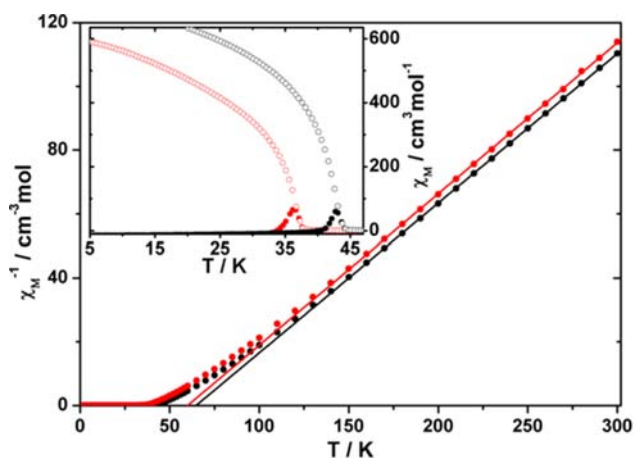

Figure 7. Thermal dependence of χ_M^{-1} with fit (solid line) for **1** (black) and **2** (red). Inset: ZFC (full symbols) and FC (empty symbols) plots for **1** (black) and **2** (red).

respectively, correspond well with the 2.11 cm³ K mol⁻¹ value expected per formula unit $Cu^{II}_3W^V_2$ assuming the isotropic g = 2.0 for M^V (M = W (**1**), Mo (**2**)) and g = 2.2 for Cu^{II}. The $\chi_M(T)$ and $\chi_M T(T)$ plots at 1 kOe are presented in Supporting Information, Figures S12−S13. The zero-field-cooled (ZFC) magnetization curves show peaks with maxima at 43 and 37 K for **1** and **2**, respectively. The field-cooled (FC) magnetization plots (H_{dc} = 10 Oe) exhibit a spontaneous magnetization with a critical temperature (T_c) of 43 and 37 K for **1** and **2**, respectively, and then the magnetization monotonically increases (Figure 7 inset).

The AC magnetic susceptibility measured at H_{ac} = 3 Oe at frequency f = 10, 100, and 1000 Hz (Figure 8) demonstrates sharp maxima in the plot of the in-phase signal (χ_M') at 43 and 37 K for **1** and **2**, respectively. The out-of-phase signal (χ_M'') have maxima at the same temperatures. The position of the χ_M' maximum does not depend on AC frequency confirming a long-range magnetic ordering.

The magnetization at 50 kOe reaches 4.6 and 4.8 Nβ for **1** and **2**, respectively (Figure 9), and still increases. These values correspond to the predicted value 5.3 Nβ for the $Cu^{II}_3W^V_2$ unit. Additionally, both compounds reveal magnetic hysteresis loop

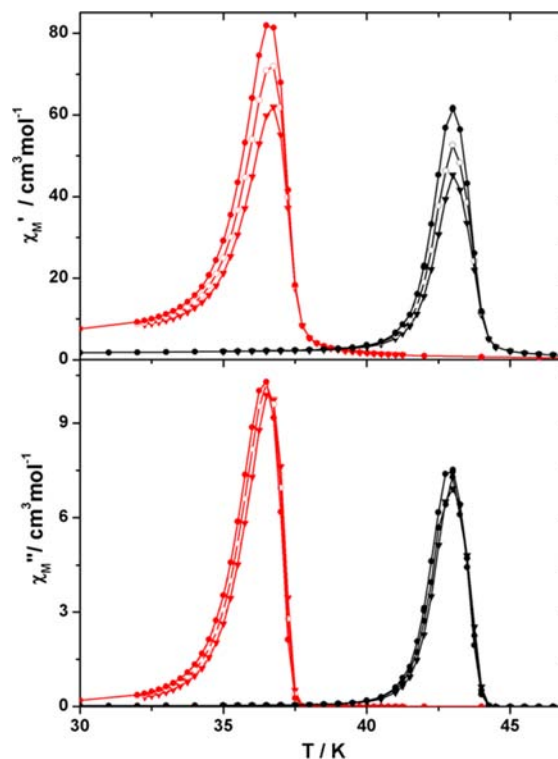**Figure 8.** In-phase χ_M' and out-of-phase χ_M'' components of AC susceptibility vs T measured at 10 (●), 100 (○), and 1000 Hz (▼) for **1** (black) and **2** (red).
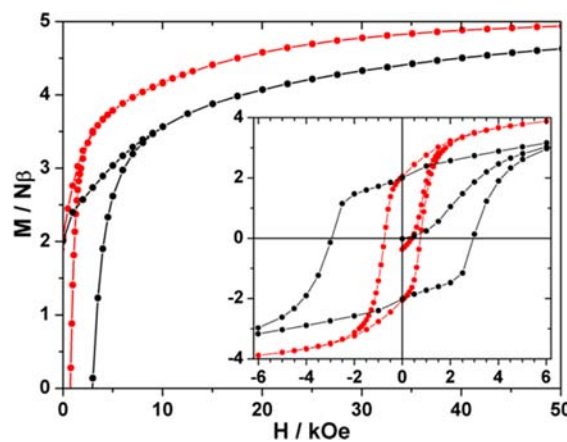

Figure 9. Field dependence of magnetization at 2 K for **1** (black) and **2** (red) with zoomed range (inset).

at 2 K with coercive field (H_{coer}) of 3.0 and 0.75 kOe for **1** and **2**, respectively.

■ DISCUSSION

The two previously reported compounds with a 3-D topology based on $\{Cu^{II}[W^V(CN)_8]^-\}_n$ double-layers linked by inter-layer copper centers exhibit long-range magnetic ordering with Curie temperature of 40 K and coercive field of 2.0 and 2.5 kOe.[4] The similar magnetic properties were obtained for **1**, which reveals ferromagnetic interaction with T_c = 43 K and coercive field 3.0 kOe. Such behavior can be explained in terms of comparable structure of **1** and **Cu$_{2.44}$W**. Our studies confirm the analogous 3-D structure modified with coordinated pyrazine. In the case of **2**, we observed a T_c value of 37 K

and coercive field reaching 0.75 kOe. The coercive field for **2** is the largest value among $Cu^{II}-Mo^{V}$ cyanido-bridged systems.[2a] The critical temperature of the long−range magnetic ordering of the octacyanidotungstate(V) based compound is about 6 K higher than of the molybdenum analogue. Similar behavior was observed for the $Mn(II)-M(V)^{17}$ and $Cu(II)-M(V)$ systems,[2a,b] where ordering temperature is higher by several degrees for M = W than for M = Mo. This observation is confirmed also by the studies of local exchange interactions in low nuclearity cyanido-bridged molecules $Ni^{II}-L-[M^{V}(CN)_8]^{3-}$ as well.[18]

Insertion of the intra-layer Cu ion bridging Cu−W double layers leads to the ferromagnetic structure contrary to antiferromagnetic interlayer interactions in nonbridged layers in the reference system.[2,3] This means that the exchange interactions through the intra-layer Cu ion is ferromagnetic and stronger than the dipolar interactions between the layers. However, the critical temperature does not increases significantly.

CONCLUSIONS

As a part of our studies aimed at the development of XAS application for the description of coordination spheres of metal centers in $Cu^{II}-[M^{V}(CN)_8]^{3-}$ systems we have correlated the XANES and EXAFS data with the molecular structure of previously reported compounds. This correlation resulted in the unique interpretation of the structure of isostructural polymers $Cu^{II}_3(pyz)[M^{V}(CN)_8]_2 \cdot xH_2O$ (M = W, x = 0 (**1**); M = Mo, x = 3.5 (**2**)) built of $\{Cu^{II}[W^{V}(CN)_8]^-\}_n$ double-layers linked by cyanido-bridged $\{Cu^{II}-(\mu\text{-pyz})^{2+}\}_n$ chains.

These $Cu^{II}-M^{V}$ systems reveal long−range magnetic ordering with T_c of 43 and 37 K for **1** and **2**, respectively. The presence of the 3-D coordination networks and high number of cyanido-bridges leads to the highest Curie temperatures among $Cu^{II}-[M^{V}(CN)_8]^{3-}$ systems with organic ligands reported so far. Moreover, these compounds exhibit the widest hysteresis loops for $Cu^{II}-M^{V}$ systems, with coercivity 3.0 and 0.75 kOe for **1** and **2**, respectively.

To the best of our knowledge the presented results are the first example of XAS−structural correlation in this class of systems.

ASSOCIATED CONTENT

Ⓢ Supporting Information

IR spectra with interpretation of **1**, **2**, and pyrazine; the interlayer distances calculated from the position of the first Bragg peak; Cu:K edge energies of measured samples; structural parameters of reference samples (tungsten and copper centers); XANES spectra for W:L₃ and Mo:K edges; the $k^3 \times \chi(k)$ functions obtained from Cu:K, Mo:K, and W:L₃ edge spectra; thermal dependence of χ_M and $\chi_M T$. This material is available free of charge via the Internet at http://pubs.acs.org..

AUTHOR INFORMATION

Corresponding Author

*E-mail: barbara.sieklucka@uj.edu.pl (B.S.), olaf.stefanczyk@uj.edu.pl (O.S.).

Notes

The authors declare no competing financial interest.

REFERENCES

(1) (a) Sieklucka, B.; Podgajny, R.; Korzeniak, T.; Nowicka, B.; Pinkowicz, D.; Kozieł, M. *Eur. J. Inorg. Chem.* **2011**, *3*, 305−326. (b) Nowicka, B.; Korzeniak, T.; Stefańczyk, O.; Pinkowicz, D.; Chorąży, S.; Podgajny, R.; Sieklucka, B. *Coord. Chem. Rev.* **2012**, *256*, 1946−1971.

(2) (a) Korzeniak, T.; Podgajny, R.; Alcock, N. W.; Lewiński, K.; Bałanda, M.; Wasiutyński, T.; Sieklucka, B. *Polyhedron* **2003**, *22*, 2183−2190. (b) Podgajny, R.; Korzeniak, T.; Balanda, M.; Wasiutynski, T.; Errington, W.; Kemp, T. J.; Alcock, N. W.; Sieklucka, B. *Chem. Commun.* **2002**, 1138−1139.

(3) Kaneko, S.; Tsunobuchi, Y.; Sakurai, S.; Ohkoshi, S. *Chem. Phys. Lett.* **2007**, *446*, 292−296.

(4) Podgajny, R.; Chmel, N. P.; Bałanda, M.; Tracz, P.; Gaweł, B.; Zając, D.; Sikora, M.; Kapusta, C.; Łasocha, W.; Wasiutyński, T.; Sieklucka, B. *J. Mater. Chem.* **2007**, *17*, 3308−3314.

(5) (a) Zentková, M.; Mihalik, M.; Arnold, Z.; Kamarád, J.; Bałanda, M.; Podgajny, R.; Sieklucka, B. *Czech. J. Phys.* **2004**, *54*, D527−D530. (b) Pełka, R.; Bałanda, M.; Wasiutyński, T.; Nakazawa, Y.; Sorai, M.; Podgajny, R.; Sieklucka, B. *Czech. J. Phys.* **2004**, *54*, D595−D598. (c) Bałanda, M.; Pełka, R.; Wasiutyński, T.; Rams, M.; Nakazawa, Y.; Miyazaki, Y.; Sorai, M.; Podgajny, R.; Korzeniak, T.; Sieklucka, B. *Phys. Rev. B* **2008**, *78*, 174409. (d) Czapla, M.; Pełka, R.; Zieliński, P. M.; Budziak, A.; Bałanda, M.; Makarewicz, M.; Pacyna, A.; Wasiutyński, T.; Miyazaki, Y.; Nakazawa, Y.; Inaba, A.; Sorai, M.; Pratt, F. L.; Podgajny, R.; Korzeniak, T.; Sieklucka, B. *Phys. Rev. B* **2010**, *82*, 094446. (e) Wasiutyński, T.; Bałanda, M.; Czapla, M.; Pełka, R.; Zieliński, P. M.; Pratt, F. L.; Korzeniak, T.; Podgajny, R.; Pinkowicz, D.; Sieklucka, B. *J. Phys.: Conf. Ser.* **2011**, *303*, 012034.

(6) (a) Rohrkamp, J.; Phillips, M. D.; Turnbull, M. M.; Lorentz, T. *J. Phys.: Conf. Ser.* **2010**, *200*, 012169. (b) Tsyrulin, N.; Xiao, F.; Schneidewind, A.; Link, P.; Rønnow, H. M.; Gavilano, J.; Landee, C. P.; Turnbull, M. M.; Kenzelmann, M. *Phys. Rev. B* **2010**, *81*, 134409. (c) Manson, J. L.; Schlueter, J. A.; Funk, K. A.; Southerland, H. I.; Twamley, B.; Lancaster, T.; Blundell, S. J.; Baker, P. J.; Pratt, F. L.; Singleton, J.; McDonald, R. D.; Goddard, P. A.; Sengupta, P.; Batista, C. D.; Ding, L.; Lee, C.; Whangbo, M. H.; Franke, I.; Cox, S.; Baines, C.; Trial, D. *J. Am. Chem. Soc.* **2009**, *131*, 6733−6747. (d) Woodward, F. M.; Gibson, P. J.; Jameson, G. B.; Landee, C. P.; Turnbull, M. M.; Willett, D. *Inorg. Chem.* **2007**, *46*, 4256−4266. (e) Das, A.; Todorov, I.; Dey, S. K.; Mitra, S. *Inorg. Chim. Acta* **2006**, *359*, 2041−2046. (f) Haddad, M. S.; Hendrickson, D. N.; Cannady, J. P.; Drago, R. S.; Bieksza, D. S. *J. Am. Chem. Soc.* **1979**, *101*, 898−906. (g) Tsunobuchi, Y.; Kosaka, W.; Nuida, T.; Ohkoshi, S. *CrystEngComm* **2009**, *11*, 2051−2053.

(7) (a) Niel, V.; Martinez-Agudo, J. M.; Muñoz, M. C.; Gaspar, A. B.; Real, J. A. *Inorg. Chem.* **2001**, *40*, 3838−3839. (b) Ohba, M.; Yoneda, K.; Agustí, G.; Muñoz, M. C.; Gaspar, A. B.; Real, J. A.; Yamasaki, M.; Ando, H.; Nakao, Y.; Sakaki, S.; Kitagawa, S. *Angew. Chem., Int. Ed.* **2009**, *48*, 4767−4771. (c) Agustí, G.; Ohtani, R.; Yoneda, K.; Gaspar, A. B.; Ohba, M.; Sánchez-Royo, J. F.; Muñoz, M. C.; Kitagawa, S.; Real, J. A. *Angew. Chem., Int. Ed.* **2009**, *48*, 8944−8947.

(8) (a) Ohkoshi, S.; Tokoro, H.; Hozumi, T.; Zhang, Y.; Hashimoto, K.; Mathonière, C.; Bord, I.; Rombaut, G.; Verelst, M.; dit Moulin, C. C.; Villain, F. *J. Am. Chem. Soc.* **2006**, *128*, 270−277. (b) Podgajny, R.; Bałanda, M.; Sikora, M.; Borowiec, M.; Spałek, L.; Kapusta, C.; Sieklucka, B. *Dalton Trans.* **2006**, 2801−2809. (c) Ma, X. D.; Yokoyama, T.; Hozumi, T.; Hashimoto, K.; Ohkoshi, S. *Phys. Rev. B* **2005**, *72*, 094107. (d) Rombaut, G.; Mathonière, C.; Guionneau, P.; Golhen, S.; Ouahab, L.; Verelst, M.; Lecante, P. *Inorg. Chim. Acta* **2001**, *326*, 27−36. (e) Yokoyama, T.; Okamoto, K.; Matsumura, D.; Ohta, T.; Ohkoshi, S.; Hashimoto, K. *J. Synchrotron Radiat.* **2001**, *8*, 913−915.

(9) (a) Dennis, C. R.; van Wyk, A. J.; Basson, S. S.; Leipoldt, J. G. *Transition Met. Chem.* **1992**, *17*, 471−473. (b) Samotus, A. *Pol. J. Chem.* **1973**, *47*, 653.

(10) Ohkoshi, S.; Machida, N.; Zhong, Z. J.; Hashimoto, K. *Synth. Met.* **2001**, *122*, 523−527.

(11) Stefanczyk, O.; Korzeniak, T.; Nitek, W.; Rams, M.; Sieklucka, B. *Inorg. Chem.* **2011**, *50*, 8808−8816.

(12) Korzeniak, T.; Desplanches, C.; Podgajny, R.; Giménez-Saiz, C.; Stadnicka, K.; Rams, M.; Sieklucka, B. *Inorg. Chem.* **2009**, *48*, 2865−2872.

(13) Macrae, C. F.; Edgington, P. R.; McCabe, P.; Pidcock, E.; Shields, G. P.; Taylor, R.; Towler, M.; van de Streek, J. *J. Appl. Crystallogr.* **2006**, *39*, 453−457.

(14) Ravel, B.; Newville, M. *J. Synchrotron Radiat.* **2005**, *12*, 537−541.

(15) (a) Wang, Z. L.; Yao, K. L.; Liu, Z. L.; Zhu, L. *Solid State Commun.* **2008**, *146*, 412−415. (b) Barquín, M.; González Garmendia, M. J.; Larrínaga, L.; Pinilla, E.; Torres, M. R. *Z. Anorg. Allg. Chem.* **2005**, *631*, 2210−2214.

(16) (a) Senel, E.; Yilmaz, V. T.; Kazak, C. *Z. Anorg. Allg. Chem.* **2008**, *634*, 419−421. (b) Leznoff, D. B.; Xue, B. Y.; Stevens, C. L.; Storr, A.; Thompson, R. C.; Patrick, B. O. *Polyhedron* **2001**, *20*, 1247−1254.

(17) (a) Wang, T. W.; Wang, J.; Ohkoshi, S.; Song, Y.; You, X. Z. *Inorg. Chem.* **2010**, *49*, 7756−7763. (b) Li, D.; Zheng, L.; Zhang, Y.; Huang, J.; Gao, S.; Tang, W. *Inorg. Chem.* **2003**, *42*, 6123−6129. (c) Li, D. F.; Gao, S.; Zheng, L. M.; Tang, W. X. *Dalton Trans.* **2002**, 2805−2806. (d) Song, Y.; Ohkoshi, S.; Arimoto, Y.; Seino, H.; Mizobe, Y.; Hashimoto, K. *Inorg. Chem.* **2003**, *42*, 1848−1856. (e) Ma, S. L.; Ma, Y.; Ren, S.; Yan, S. P.; Cheng, P.; Wang, Q. L.; Liao, D. Z. *Cryst. Growth. Des.* **2008**, *8*, 3761−3765.

(18) Visinescu, D.; Desplanches, C.; Imaz, I.; Bahers, V.; Pradhan, R.; Villamena, F. A.; Guionneau, P.; Sutter, J. P. *J. Am. Chem. Soc.* **2006**, *128*, 10202−10212.